Uncovering the magnetic and electrical properties of (Fe0.65Co0.35)100-xNbx alloys for x<1

Matheus Marinho Arruda, Fernando Froes, Olivier Hubert, Cristina Bormio-Nunes

Uncovering the magnetic and electrical properties of $(Fe_{0.65}Co_{0.35})_{100-x}Nb_x$ alloys for $x < 1$.

Matheus Marinho Arruda, Fernando Froes, Olivier Hubert, Cristina Bormio-Nunes

Universidade de São Paulo (USP), Escola de Engenharia de Lorena (EEL), Departamento de Engenharia de Materiais – Area 2, Lorena, Sao Paulo, 12.612-550, Brazil

Abstract

In the interest of improving the applicability of FeCo alloys as soft magnets and closing gaps in previous studies, additions of 0.5 and 0.7 (in mass percentage) of Nb are evaluated for $Fe_{65}Co_{35}$ alloy (mass %) in terms of mechanical, magnetic and electric properties. Arc melted and cold rolled samples show an expected increase in deformation performance, the main hurdle of the binary alloy. Arc melted and hot rolled sheets reveal microparticles produced by the Nb additions, increases in the magnetic permeability and coercivity, generally maintaining the original softness of the binary material. Nb additions results in saturation magnetostriction values of around 40 ppm. Decreases smaller than 6% in the saturation polarization are reported at room temperature. A significant and unexpected reduction in the resistivity was found for the 0.7% Nb addition to the $Fe_{65}Co_{35}$ alloy, while the 0.5% Nb addition retains a resistivity value in the usual range. Both additions can result in viable soft magnetic materials, which are less expensive than the commonly used equiatomic alloy due to a decrease in the Co amount and have the potential for further improvements of their softness and magnetostriction through slight changes in the fabrication process.

Keywords: FeCoNb, Soft magnet, Magnetic properties, Magnetostriction

Introduction

Soft magnetic materials (SMM) are a class of materials known to pursue a thin hysteresis loop, meaning that they have a relatively easy capability to be magnetized and demagnetized, and low energy amounts are spent during this process. The width of the hysteresis is controlled by the coercive field H_c and as small is H_c, thinner is the hysteresis. This characteristic leads to valuable applications with growing interest such as AC and DC electric motors, generators and transformers. The equipment's part which uses the soft magnetic material is the magnetic core. Such cores enhance the magnetic field produced by a cooper electromagnet and are responsible for producing torque, by means of magnetic forces. An important requirement to reach high magnetic forces is that the magnetic material must have a high magnetic flux density (B), because the torque of motors is proportional to B^2. (Beckley, 2001)

Concerning applications in alternate current, it is also necessary to have a high magnetic permeability (low magnetic anisotropy) occurring at small magnetic fields to achieve cyclical changes fast. Another relevant magnetic property for AC applications is the magnetostriction (λ). Large λ values are not desirable since it causes noise, the humming sounds that can be heard near transformers, and some sort of heating. (Belahcen, 2006) (Zhang et al., 2021) On the other side, high magnetostriction values are exploited mainly as force sensors and actuators, as well as energy harvesters. (Kurita et al., 2023) (Khomenko et al., 2023) (Yamazaki et al., 2022)

Other applications of the soft magnetic materials (SMM) include nanowires for data storage, magnetic sensors and spintronic devices. (Gutfleisch et al., 2011) (Xu et al., 2024) FeCo based alloys fit in the SMM class. They have high polarization saturation, as large as 2.45 T and Curie temperature in the range of 920 to 985 ºC, much superior by comparing to pure Fe and Fe binary alloys. (Sundar and Deevi, 2004).

The commercially available alternatives of Fe-Co alloys are quasi-binary alloys which are mostly

restricted to Hiperco® 27 (27% Co, 0.6% Ni and Cr, 0.25% Mn and Si, 0.01% C; mass %) (Carpenter Technology, a) and Hiperco® 50 (48.5% Co, 0.01% C, 0.0.5 % Mn, 0.0.5 % Si, 0.0.5 % Nb, 1.90% V; mass %) (Carpenter Technology, b). Improved magnetic properties can be obtained through magnetic or under stress annealing of those alloys.

Hiperco®27 hot rolling can be performed from 1177°C down to 927°C, but it does not suffer from the worse ductility of Hiperco®50. However, Hiperco®27 has a poorer magnetic permeability compared to Hiperco®50. Considering the complex composition of the commercial alloys, it is not possible to understand the effect of each element on the magnetic properties of the alloys. The study of the effect of each element addition individually on the magnetic properties of the binary Fe-Co alloy is motivating, because the understanding of the origin of the improvement or degradation of the magnetic properties of the Fe-Co alloys can help the development of optimized alloys on a scientific basis. Moreover, there is an interest in reducing the amount of Co amount in Fe-Co alloys below 50% because the Co is significantly more expensive than the iron, around 329 times. (TRADING ECONOMICS, 2025)

Therefore, it is of interest to increase the permeability of lower Co amount in FeCo alloys maintaining good ductility.

The obstacle of brittleness of high Co content alloys occurs between 28% to 73% of Co and is associated with α'-phase presence, an ordered BCC phase with B2 structure (Ohnuma et al., 2002). This phase appears on the alloy cooling and the ordering temperature depends on the Co content, ~ 730°C in 50%Co alloy and 690°C in 35% Co alloy. This fragility is generally mitigated by alloying elements, such as V in Hiperco®50, with various other elements such as C, Cr, Ti, Ni, Nb, Ta and B showing similar improvements. (Kawahara, 1983) (Froes, 2021) Their effect is most notably in stabilizing the α-phase with A2 structure at the cost of saturation magnetization reduction, and in forming Co_3X clusters. (Kawahara, 1983) (Sundar and Deevi, 2005).

The binary alloy with 35% of Co of has the maximum saturation polarization among all Fe-Co alloys and has intermediary values of coercivity and permeability which are higher than 27% of Co, but lower than 50% of Co alloys. (Sundar and Deevi, 2005) (Gutfleisch et al., 2011) In addition, the magnetostriction decreases for decreasing Co content in Fe-Co alloys in the range of 50% to 27%. One direction of enhancing magnetic permeability is by inducing favorable textures during the fabrication processes, for example by the material rolling to sheets as well as magnetic and stress annealing. This route requires the material to be easily deformed, that can be achieved by introducing alloying elements. (Kawahara, 1983) Consequently, favorable textures as and magnetic and stress annealing can be engineered, and the magnetic permeability improvement would be achieved. (Dias et al., 2015)

In the case of Nb addition to Fe-Co (1:1) equiatomic alloy, there are also meaningful contributions from reducing grain size by forming secondary phases, due to Nb diminished solubility because of its large atomic radius, 146 pm, when compared to Fe (126 pm) and Co (125 pm). (Kawahara, 1983) (Sundar and Deevi, 2005) In addition, a recent theoretical work shows that Nb additions could lead to an improvement in stress accommodation via slip band formation within grains, which hampers the development of microcracks. (Muralles et al., 2024)

In this sense, with the purpose of obtaining good ductile material and searching for a higher magnetic permeability compared to the binary alloy, niobium additions to the alloy with 35% of Co (in mass) are evaluated in this study. The amount of Nb added 0.5% and 0.7% was aimed for complete solubility in the Fe-Co alloy. Promising previous results for the addition of Nb to a 30% Co alloy resulted in large increases not only in the malleability, but also in the magnetic softness of the alloy. Moreover, the addition of Nb also increases the material resistivity and reduced the magnetostriction. (Bormio-Nunes and Froes, 2023) (Froes and Bormio-Nunes, 2024) In the case of the resistivity, the increase is interesting for limiting eddy currents and subsequently energy losses in AC applications, which is likely explained by the presence of secondary phases and distortions in the crystal lattice caused by

the diluted Nb. The difference in properties between the binary alloys with 30% and 35% of Co is that the second alloy has intrinsically a higher magnetic permeability (lower magnetic anisotropy) and a smaller lattice parameter.

Materials and Methods

Two alloys were studied in the present work, namely, $(Fe_{0.65}Co_{0.35})_{100-x}Nb_x$ for x = 0.5 and 0.7, in which x is the mass %. For each alloy four ingots of 40 g were prepared with the employment of high purity materials (99.8% for Fe, 99.93% for Co and 99.9% for Nb). These components were then melted in an arc furnace in an inert atmosphere. To ensure good homogeneity, 5 steps of melting were performed and afterwards a homogenization annealing at 1200 ºC for 6 hours was concluded with a quenching in water.

Samples containing 0.5% of Nb were designated as 0.5% Nb, whilst those with 0.7% of Nb as 0.7% Nb. Four alloys of each composition were produced.

One alloy of each composition went through 3 steps of cold rolling to evaluate their malleability. In each stage, including before the first rolling, small pieces were extracted from them for Vickers hardness tests in a BUEHLER MICROMET 2004 hardness tester. The procedure for all pieces was 10 measurements with a force of 100 kgf during 15 s. Grinding silicon carbide papers with grit sizes ranging from P320 to P2500 were used to polish the samples' surfaces.

The remaining alloys underwent multiple hot rolling steps, at 1100 ºC, until reaching the desired thickness. Subsequently, they were cut into rectangular sheets shapes and were annealed at 800 ºC-for 6 hours followed by quenching to retain the disordered magnetic BCC phase.

For these alloys, composition data was gathered from Energy Dispersive X-ray Spectroscopy (EDS)

with a Hitachi-4000 scanning electron microscope (SEM) equipped with an EBSD detector from EDAX and an EDS detector from Oxford. A minimum of 5 points per sample was analyzed for an average result. Furthermore, from 0.5% Nb and 0.7% Nb, backscattering images were obtained to study the grains morphology and sizes, and to identify a possible presence of second phases in the materials. The scans were performed in representative areas of 500 μm × 500 μm for grains size. The metallographic preparation was a sequence of grinding papers, polishing with aluminum and silicon oxides solutions, ultrasonic cleaning and finalized in a Vibromet – Buehler to remove the surface stresses induced in the grinding and polishing process. EBSD analysis was also performed in smaller areas of 100 μm × 200 μm to help with the quantification of the second phase volume fraction and using a standard disordered BCC pattern and a Laves C14 pattern. (Varli et al., 1981)

To evaluate the phases, XRD analysis was performed in powder samples of 0.5% Nb-1 and 0.7% Nb-1 in a diffractometer Empyrean from PANanalytical with Mo-Kα radiation. The data was analyzed using the Powder- Cell program. (Varli et al., 1981)(Hocine et al., 2017)

Magnetic properties were accessed first by subjecting sheets of 0.5% Nb-3 and 0.7% Nb-3 to 10 hysteresis cycles with external magnetic fields ranging from - 11 kA/m to 11 kA/m. Magnetostriction measurements were also carried out with a gauge measuring transversal deformation and 2 gauges giving the average for the longitudinal deformation.

The magnetic saturation and resistivity were attained as functions of temperature in the ranges of 2 K and 900 K and 2K to 350 K, respectively, in a Physical Properties Measuring System (PPMS) from Quantum Design. For the first, samples of around 3 x 3 x 2 mm were employed. Meanwhile, for the resistivity, samples of around 0.1 to 0.2 mm of thickness and 1 mm of width were used, resulting in transversal areas of between 0.1 and 0.2 mm². The length between the voltage contacts, taking into account the four-point method, was between 2 and 4 mm.

1. Results and discussion

1.1. Microstructure

The samples phases and grains boundaries observed by SEM/EBSD of the RD-TD faces of the $Fe_{65}Co_{35}$ with 0.5% Nb - 1 and 0.7% Nb - 1 alloys can be seen in Figure 1 (a-b). It is possible to observe the grains boundaries as well as the second phase, indicated by arrows and white in color, that second phase tends to gather mostly on the grain boundaries for the 0.5% Nb alloy. For the 0.7% Nb alloy, the second phase also develops at grain boundaries, but small grains grow at triple points and as isle grains inside a large grain. In addition, the second phase is denser in the 0.7% Nb alloy grain boundary. After observing many areas, the second phase quantification resulted in 0.2% of the second phase for the 0.5% Nb alloy and 0.6% for the 0.7% Nb alloy.

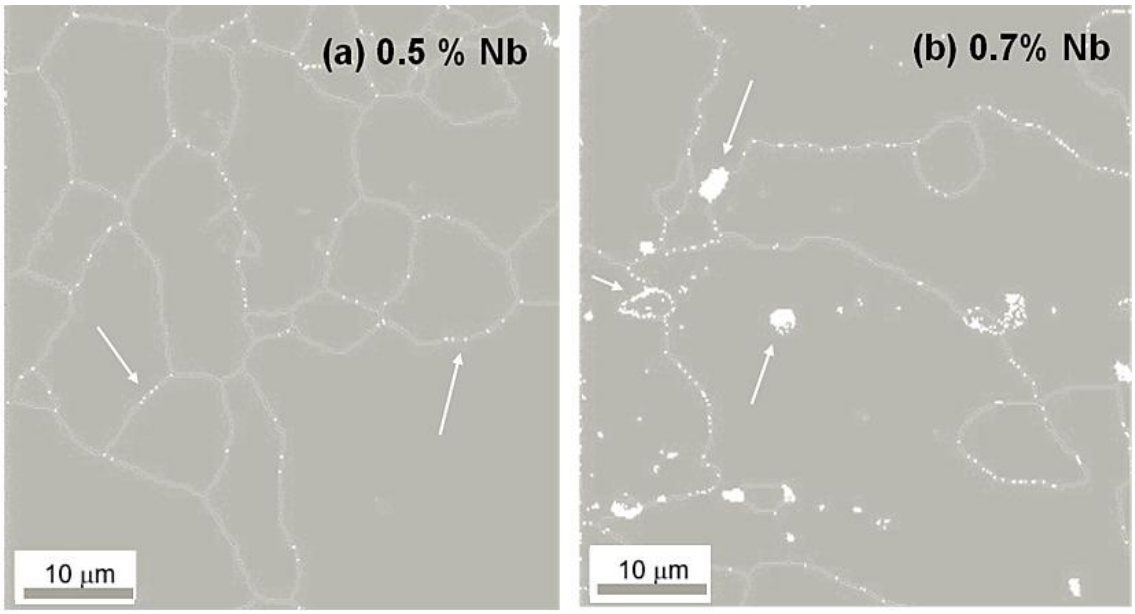

Figure 1: SEM/EBSD phases results on the RD-TD faces of $Fe_{65}Co_{35}$ - 0.5% Nb - 1 and 0.7% Nb - 1 alloys. The arrows denote some positions of the second phase.

The complete EBSD analysis was made in the rolling (RD), normal (ND) and transverse (TD)

directions of the sheet on the alloys 0.5 % Nb – 1 and 0.7 % Nb - 1, corresponding in this sequence to the surfaces ND-TD, RD-TD and RD-ND. The grains structures for both alloys are shown in colored Figure 2. In grey tons is the picture of the Image Quality (IQ).

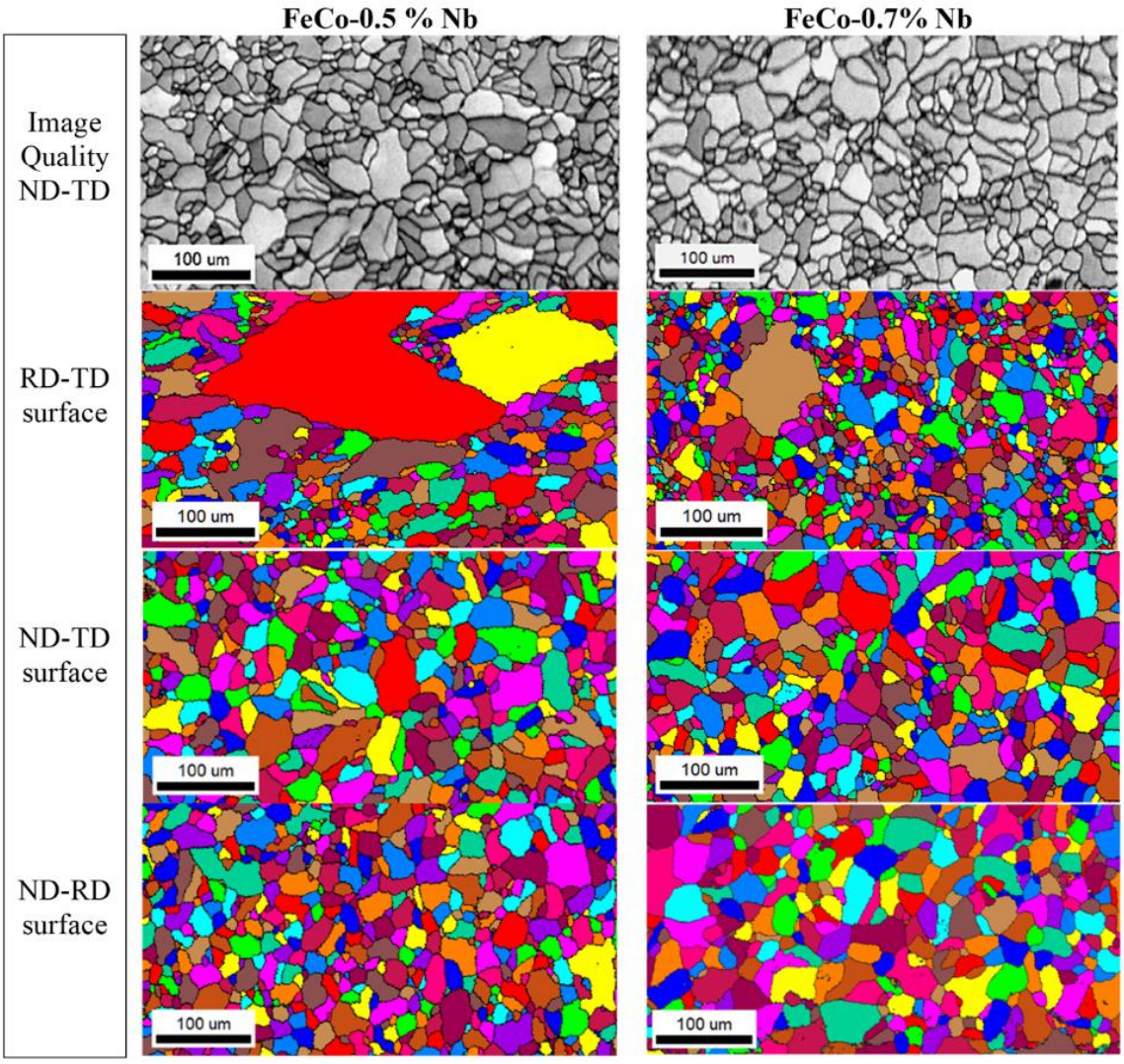

Figure 2 - EBSD analysis of the 0.5 % Nb - 1 and 0.7% Nb - 1 alloys on the sheet surfaces ND-TD (RD direction), RD-TD (ND direction) and RD-ND (TD direction).

Figure 3 depicts the grains areas fractions as a function of the grain's sizes graphs for both alloys' compositions and in Table 1 the values of the grains mean sizes for each surface and the mean grain sizes of each alloy calculated averaging the sizes of the three surfaces, since the area analyzed were the same for each surface.

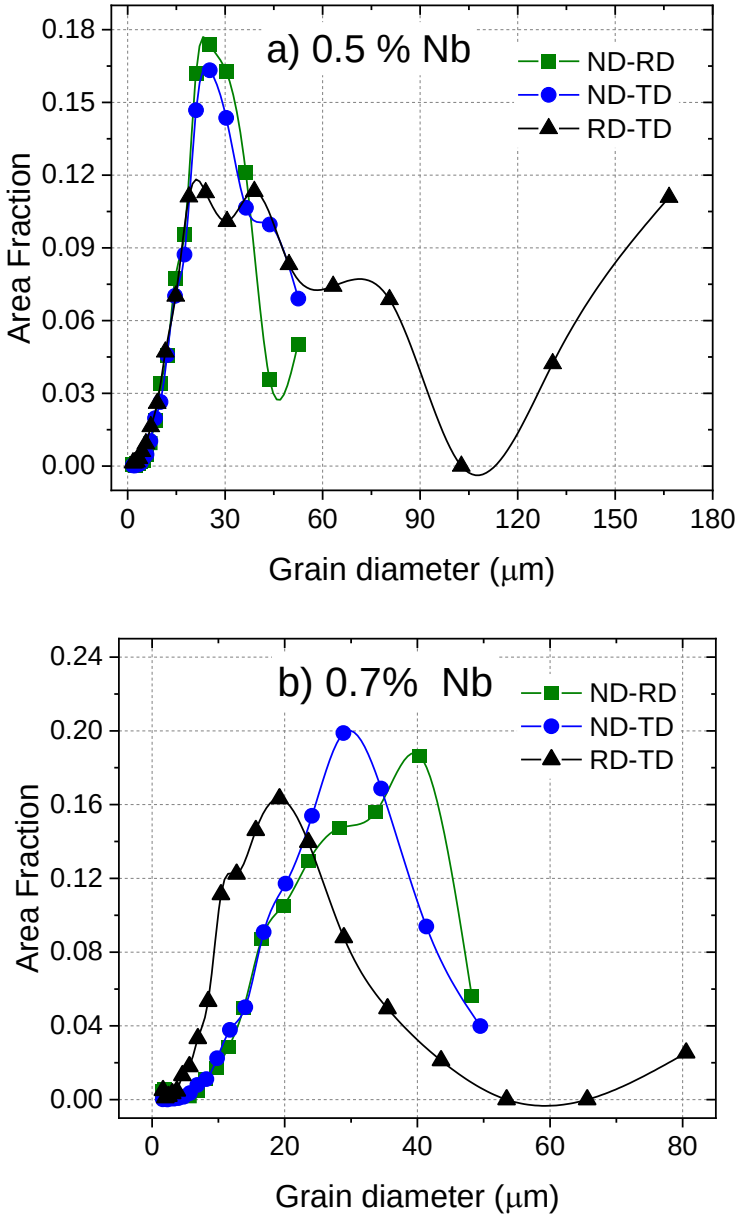

Figure 3 - Area fraction as a function of the grain's sizes results for 0.5 % Nb - 1 and 0.7% Nb - 1 alloys in the ND (RD-TD surface), RD (ND-TD surface) and TD (ND-RD surface) directions.

Table 1 shows that as Nb addition to $Fe_{65}Co_{35}$ increases from 0.5% to 0.7%, grain refinement takes place, confirming the role of Nb in small amounts as inhibitors of grain growth, similarly to Zr and V (Sundar et al, 2005). In the ND direction, this refinement is more obvious since in the TD and RD directions the grains sizes are almost the same for both alloys. In both alloys, for all the surfaces, a clear larger area fraction of grains occurs for grain sizes (D) in the range of 20 to 40 μm. However,

RD-TD surface of 0.5 % Nb alloy shows more two maximum areas at D ~ 75 μm and D ~175 μm, while 0.7% Nb alloy RD-TD surface shows a tendency of areas fraction growing for D > 80 μm. These findings point to abnormal grain growth (AGG) in the 0.5 % Nb alloy, noticeable in the RD-TD surface. Conversely, in 0.7% Nb alloy the AGG is not so obvious. A recent study in Fe-Ga alloys shows that nanometric particles are effective in provoking AGG, which may also be the case for the small particles present in 0.5% Nb (He et al., 2021).

Table 1 - Values of the grains mean sizes for each surface, RD-TD, ND-TD and RD-ND and the mean grain size values of each alloy

SURFACE - grains sizes mean value (μm)				
ALLOY	RD-TD	ND-TD	ND-RD	Overall grain mean size (μm)
05 Nb	52.7 ± 0.8	27.1 ± 1.7	25.7 ± 1.7	35.2 ± 4.4
7 Nb	19.6 ± 1.2	26.6 ± 2.0	27.6 ± 2.1	24.6 ± 5.3

To have a clue of the second phase crystallographic structure, thermodynamic calculations were performed in the Thermo-Calc program with the use of an iron database, with the resulting phase distribution per temperature shown in Figure 4 only for the 0.5% Nb alloy. No meaningful difference between the two compositions was found, and the second phase was identified as being a hexagonal phase, Laves C14 of composition $(Fe\text{-}Co)_2Nb$, space group $P6_3/mmc$ (194). (Varli et al., 1981) Furthermore, at room temperature, the calculated amount of this second phase in volume fraction is 1.1% for 0.5% of Nb additions and to 1.4% for 0.7% of Nb additions to the $Fe_{0.65}Co_{0.35}$ alloy, with minor variations until the phase transition. The calculated volume fractions of the second phase are larger than observed by EBSD analysis. This difference may be since the particles are not apparent on the scale at which they were observed, thus exists more particles on a smaller scale. In addition, in the

RD-TD surface in which the second phase was observed (Figure 2) the grains are larger than in the ND-TD and ND-RD surfaces, leading to a shorter grain boundaries overall length of the RD-TD surface, resulting in less second phase quantity. Therefore, the quantification of the area fraction extrapolation of the volume fraction in this case does not give a reasonable estimation, because the microstructure is anisotropic.

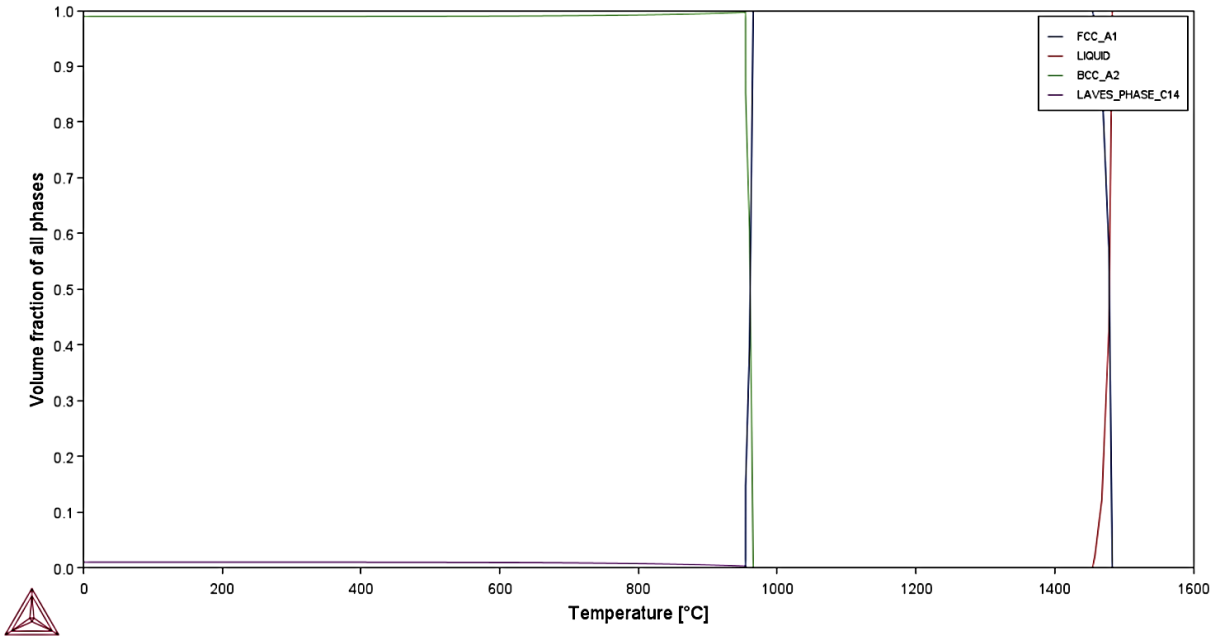

Figure 4: Thermo-calc calculation of phase volume fraction as a function of the temperature for the 0.5 % Nb alloy $(Fe_{0.65}Co_{0.35})_{99.5}Nb_{0.5}$.

Figure 5 shows the XRD patterns of the $Fe_{0.65}Co_{0.35}$ alloys added with 0.5% of Nb and 0.7% of Nb, with the crystallographic orientation of each peak of the main phase (BCC) and indications of the presence of the second phase (Laves). The XRD profiles were analyzed using PowderCELL program (Hocine et al., 2017) (Varli et al., 1981), using a standard pattern of BCC $Fe_{0.7}Co_{0.3}$ alloy as reference for the matrix and of standard Laves ($MgZn_2$ type) $(Co_{0.75}Nb_{0.25})_2Nb$ for the second phase. The two more intense $(Co\text{-}Fe)_2Nb$ (Laves) XRD intensities are at $2\theta = 18.4^{o}$ and 19.9^{o}, therefore the

peak observed at 2θ = 18.1º, for both alloys, may correspond to this phase, and it is expected that the one at ~ 20º is convoluted with the peak (110) of the BCC phase.

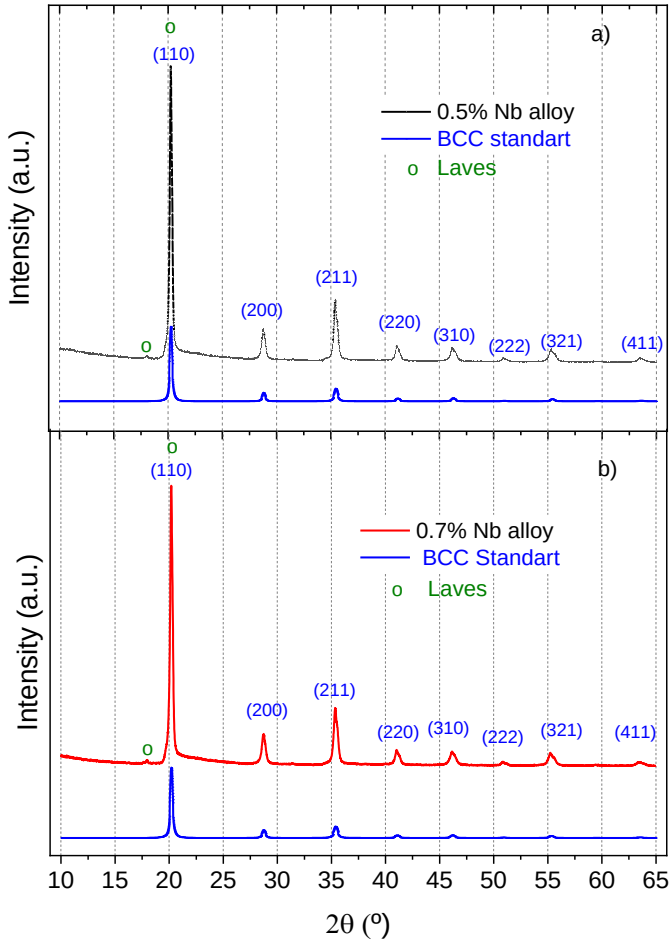

Figure 5 - XRD patterns of the $Fe_{0.65}Co_{0.35}$ alloys added with 0.5% Nb and 0.7% Nb.

The alloy $Fe_{0.65}Co_{0.35}$ without Nb has a lattice parameter of a = 2.8595 Å (Silva et al., 2024). For 0.5 % Nb – 1 and 0.7 % Nb – 1, the resulting parameter were 2.8557 Å and 2.8576 Å respectively. Given that the atomic radius of Nb is larger than those of Fe and Co, the unexpected decrease noticed for the first alloy can be related mainly to the proportion of iron to cobalt in the matrix. As presented in the following EDS results, the niobium is almost not present in the matrix and the percentage of iron, with a slightly larger radius than Co, in relation to cobalt grows from the 0.5 % addition to the 0.7 %, with both smaller than the binary alloy.

As mentioned in the Materials and Methods section, four alloys of each composition were produced,

and Table 2 presents the EDS analysis results of all those alloys matrix. All the alloys have just about the nominal composition. The composition calculated standard errors of the matrix away from the precipitates are a maximum of 0.2% for the 3 elements Nb, Fe and Co. In addition, the differences of elements contents among each ingot of the same composition are negligible.

Table 2 - EDS analysis of the matrix, away from the precipitates for the four alloys produced.

Alloy	Nb	Fe	Co
Nominal (0.5% Nb)	0.5	64.675	34.825
0.5% Nb-1	0.495	64.847	34.658
0.5% Nb-2	0.495	64.538	34.964
0.5% Nb-3	0.507	64.601	34.892
0.5% Nb-4	0.519	64.661	34.819
Nominal (0.7% Nb)	0.7	64.545	34.755
0.7% Nb-1	0.71	64.59	34.69
0.7% Nb-2	0.70	64.63	34.67
0.7% Nb-3	0.70	64.56	34.73
0.7% Nb-4	0.72	64.64	34.64

In addition, Table 3 shows the alloys 0.5 % Nb-1 and 0.7% Nb-1 points' analysis close to the precipitates and on the particulate, trying to bring some insight to the understanding of the characteristics of the second phase on these alloys.

Table 3 – EDS analysis of points closes to the precipitates and on the particulate.

Alloy	Matrix near the precipitate		
	Nb	Fe	Co
0.5% Nb	0.103	63.52	36.38
0.7% Nb	0.112	65.05	34.84
	Precipitate		
	Nb	Fe	Co
0.5% Nb	7.832	57.58	34.59
0.7% Nb	11.98	55.55	32.46

Since the particles' sizes are about to the EDS technique's dimension resolution, the result does not

have good precision and the standard errors are much larger than the measurements made on the matrix. The maximum error in the Nb content near the matrix is 37%, inside the precipitate is 6% and 2% for Co and Fe on both places. Although qualitative, the reduction of Nb in the matrix near the precipitates is clearly observed, as well as the enrichment of Nb in the precipitate.

1.2. Mechanical properties

The 0.5% Nb and 0.7% Nb samples went through three cold rolling steps, the material's fracture was achieved at roughly at 39% of deformation for the 0.5 % Nb alloy and above 52% of deformation for the 0.7% Nb alloy. The average Vickers microhardness test results for samples of both alloys collected after each rolling step are presented in Figure 6, in which the lines are only guide to the eyes. There is technically almost no difference between 0.5 % Nb and 0.7% Nb alloys strain hardening for similar deformations. However, the significant increase in ductility of 0.7% Nb compared to 0.5 % Nb alloy is also in accordance with Bormio-Nunes and Froes (2023) and Kawahara (1983). The decreasing of the alloy brittleness with increasing Nb content may be related to Nb stabilization of the disordered BCC phase.

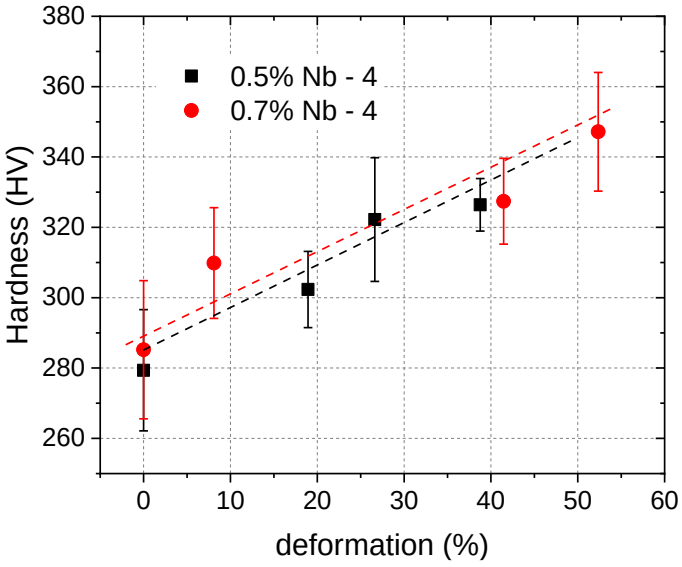

Figure 6: Vickers hardness results for $Fe_{0.65}Co_{0.35}$ alloy with addition of 0.5% Nb and 0.7% Nb for increasing steps of cold rolling deformation.

1.3. Magnetic Properties

The magnetic properties of the $Fe_{0.65}Co_{0.35}$ alloy with Nb additions of 0.5% and 0.7% were performed in alloy 3 (see Table 2). Hysteresis and the relative permeability curves are presented in Figure 7 (a-b). Those measurements reveal that both Nb additions of 0.5% and 0.7% resulted in materials with similar hysteretic characteristics. But the initial magnetic inductions are not so close, and a meaningful difference can be noticed in Figure 7 (b) for the relative permeability, in magnitude and the magnetic field value at which the maximum permeability takes place.

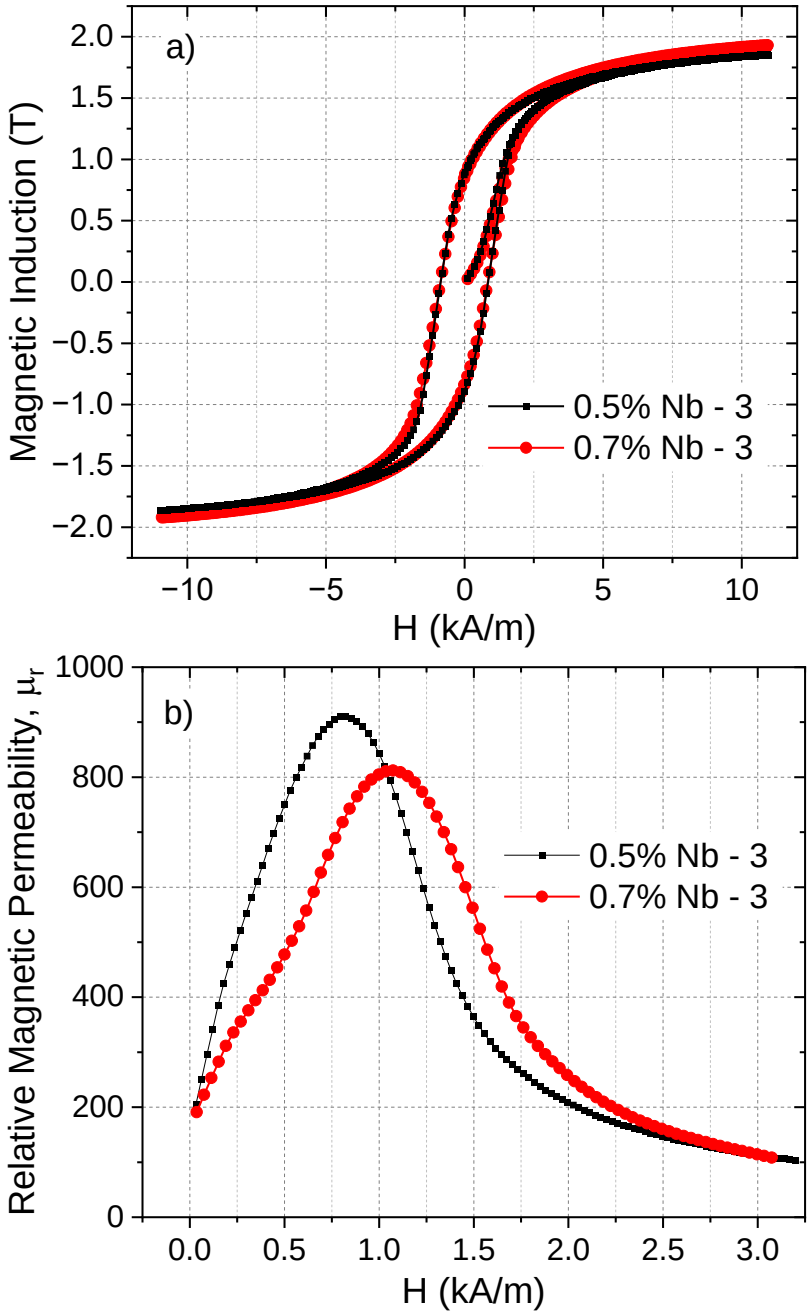

Figure 7 - $Fe_{65}Co_{35}$ alloys with addition of 0.5% Nb-3 and 0.7% Nb-3: (a) magnetic induction and (b) the relative magnetic permeability, as a function of the applied magnetic field.

The coercive field, the remanent induction and the initial and maximum permeabilities data of the $Fe_{0.65}Co_{0.35}$ alloy with 0.5% and 0.7% of Nb additions, got from the hysteresis shown in Figure 7(a) are presented in Table 4.

Table 4 – Magnetic properties: B_r (remanent induction), H_c (coercive field), initial and maximum susceptibilities (χ_i and χ_{max}) of the 0.5 % Nb and 0.7% Nb alloys.

Property	**0.5% Nb - 3**	**0.7% Nb - 3**	**$Fe_{65}Co_{35}$**
B_r (T)	0.987	1.056	-
H_c (A/m)	847	727	-
χ_i	569	239	300 (Sundar and Deevi, 2005)
χ_{max}	914	813	200 (Sundar and Deevi, 2005)

The B_r values are barely the same for both alloys, whilst 0.7% Nb alloy H_c is smaller than that of the 0.5 % Nb alloy. Additionally, χ_i and χ_{max} have opposite trends, 0.5 % Nb alloy χ_i is the highest while 0.7% Nb alloy χ_{max} is the highest. The maximum permeability increased considerably for both alloys.

The significant smaller H_c value of the 0.7% Nb compared to the 0.5% Nb alloy is unexpected, because the 0.7%Nb alloy has more second phase particles than the 0.5% Nb alloy. Therefore, as grain boundaries and second phases are in general effective domain wall pinners (Cullity, 2009) and alloy 0.7% Nb has also smaller mean grain size value than 0.5 % Nb alloy, or a large area of grain boundaries, H_c value of the 0.7% Nb alloy would be expected to be the highest. Respect to the magnetic properties of the precipitates, studies of $(Fe_{1-x}Co_x)_2Nb$ alloys for $x \leq 0.55$ revealed that they are weak ferromagnets with $T_C < 35$ K (Paduani et al., 2009), therefore those precipitates are paramagnetic at room temperature. One possibility is that ordering may be playing some hole in the pinning of domain walls as will be evidenced with M vs T results.

Figure 8 exhibits the magnetostriction curves for both compositions, 0.5 % Nb and 0.7% Nb alloys by applied field H (kA/m).

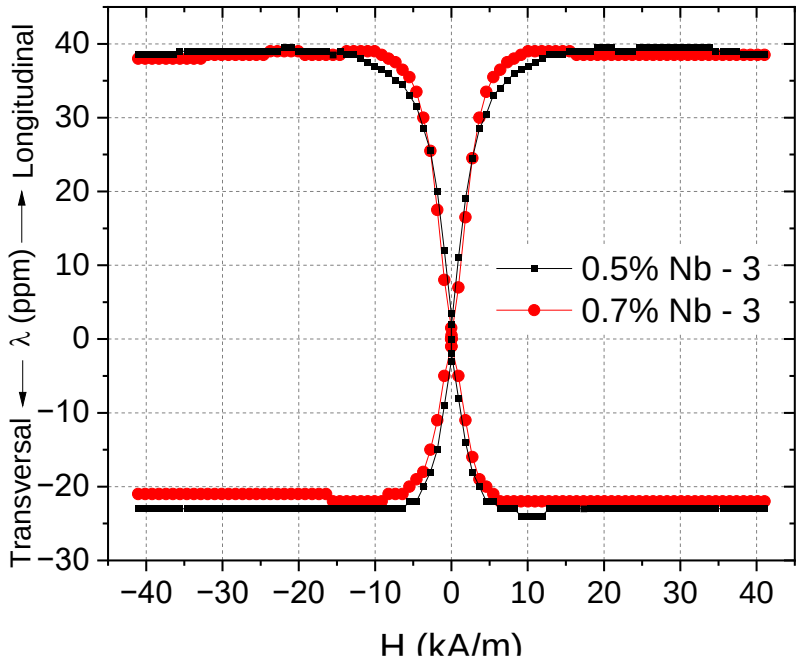

Figure 8 - Magnetostriction curves for the $Fe_{65}Co_{35}$ alloy with addition of 0.5% Nb and 0.7% Nb.

The magnetostriction values at the saturation are presented in Table 6, and the error associated is roughly 1 ppm. To obtain the saturation magnetostriction λ_s the relation $\lambda_{total} = \lambda_{long} - \lambda_{trans} = (3/2)\lambda_s$ was used. The data for the binary alloys are also presented for comparison. (Han et al, 2017)

Table 6: Values of λ_{long} and λ_{trans} taken at saturation for the $Fe_{0.65}Co_{0.35}$ - 0.5% Nb and 0.7% Nb alloys. The calculated values of λ_s and λ_{total} are calculated using $\lambda_{total} = \lambda_{long} - \lambda_{trans} = (3/2)\lambda_s$.

Sample	λ_{long}	λ_{trans}	λ_{total}	λ_s
0.5% Nb-3	39	-22	61	41
0.7% Nb-3	39.5	-23.5	63	42
$Fe_{65}Co_{35}$ (Han et al, 2017)	-	-	65	43
$Fe_{50}Co_{50}$ (Han et al, 2017)	-	-	100	68

From Figure 8 and Table 6 there is a slight difference between magnetostrictions of alloy without Nb (Han et al, 2017) and the 0.5% Nb and 0.7% Nb added alloys, within the measurement error. However, by comparing λ_s values with the binary equiatomic alloy the value is small, which is desirable for application as magnetic nucleus on electric machines such as A.C motors and transformers, causing a reduction of noise that could be generated. Nevertheless, even though the magnetostriction was reduced compared to the equiatomic alloy, it is still high, indicating that the FeCo - Nb added alloys may have a high magnetoelastic coupling. An upcoming publication will discuss the piezomagnetic behavior of those materials, particularly their applications in force sensors.

1.4. Magnetization and Resistivity as a function of temperature

The 0.5 % Nb and 0.7% Nb alloys' measurements of the saturation magnetization M_s as a function of temperature were performed in the interval of 300 K to ~ 1000 K under an applied magnetic field of 1.5T and are presented in Figure 9 (a-b). The measurement starts by heating the samples and as the temperature reaches ~ 1000K the heater of the equipment is turned off and the sample cools in the inertia of the sample chamber very slowly**.** The heating curve (HC) brings information about the initial microstructure of the samples, which were quenched from 850 ºC, and retains a microstructure that is out of equilibrium. In the other side, the cooling curves brings information of the phase transformations in an equilibrium context, since the cooling is very slow. For both alloys there is hysteresis between the HC and the CC. The hysteresis is larger for the 0.5% Nb than for 0.7% Nb alloy, meaning that there is a difference between the initial microstructures of the alloys. For example, at 600 K, the magnetization cooling curve (CC) gives M_s value of 242.04 A.m²/kg for 0.5% Nb and M_s = 241.83 A.m²/kg for 0.7% Nb alloys. The difference is only 0.21 A/m², in which the smaller magnetization of the 0.7% Nb alloy is coherent with the higher quantity of Nb, a nonmagnetic atom. On the other hand, at the same temperature, by comparing the M_s heating curves (HCs) values of 0.5% Nb and 0.7% Nb

alloys, $M_s^{0.5\ \%\ Nb}$ = 240.06 A.m²/kg is a bit lower than $M_s^{0.7\%\ Nb}$ = 240.69 A.m²/kg. In another form, $M_s^{0.5\ \%\ Nb}$(HC) < $M_s^{0.7\%\ Nb}$(HC) an opposite trend observed for CCs, in which $M_s^{0.5\ \%\ Nb}$(CC) > $M_s^{0.7\%\ Nb}$(CC). In principle the quenching of the alloys at 800°C should retain only the disordered phase, but the samples may have a mixture of ordered α' (B2) and disordered α (A2) fractions of these BCC phases. As the temperature is increased from 300K, part of the α (A2) phase retained in the quenching transforms to α' (B2) until the temperature reaches the order disorder temperature transition $T_{O\text{-}D}$. Above $T_{O\text{-}D}$ only the α (A2) phase is present up to 1000K. One argument for the existence of the hysteresis between HCs and CCs could be attributed to the higher magnetic moment of the ordered phase compared to the disordered for the alloy with 35% of Co as stated by Bardos (1969). However, some features should be seen in the CC curve at $T_{O\text{-}D}$ during the cooling if the magnetic moments were different, but nothing was observed. Another argument for the existence of hysteresis could be related to a magnetomechanical effect since the quenching of the samples may have introduced internal tensions in the alloy's lattices. Materials that have positive magnetostriction show growth of the magnetization under tractive forces applied in the direction of the applied field, while under compressive forces the magnetization decreases (Cullity, 2009). Based on this behavior, as $M_s^{0.5\ \%\ Nb}$(HC) < $M_s^{0.7\%\ Nb}$(HC), a compressive tension may have been developed between ordered and disordered phases inducing deformations of the lattice $\varepsilon_{O\text{-}D}$. This analysis suggests that interfaces between ordered and disordered phases are higher for the 0.5% Nb alloy, consequently a higher fraction of ordered phase would be present in this alloy. Thus, 0.7% Nb alloy has less ordered phases than 0.5% Nb alloy. As the temperature increases in HC regime, these compressive forces are completely released above $T_{O\text{-}D}$ at which the fraction of ordered phase transforms into disordered. The determination of $T_{O\text{-}D}$ is at the point at which the HC and CC meet, 869 K (596 °C) for the 0.5% Nb and 855 K (582 °C) for the 0.7% Nb alloys. The order-disorder transition temperature decreases with the increasing amount of Nb and decreases significantly with respect to the binary alloy that has $T_{O\text{-}D}$ ≈ 943 K (670°C) that may indicate that as more Nb is added, less ordering appears. (Ustinovshikov et

al, 2006)

With this result it is possible to explain the lower value of H_c of the 0.7% Nb compared to the 0.5%Nb alloy. The H_C values are a result of the pinning forces of domain wall pinners: second phase (SP), grain boundaries (GB) and deformations $\varepsilon_{O\text{-}D}$. We suggest that SP and GB are much less effective domain wall pinners than $\varepsilon_{O\text{-}D}$, and since 0.7% Nb alloy has lower quantity of phase ordering, this material has lower H_c value compared to the 0.5% Nb alloy.

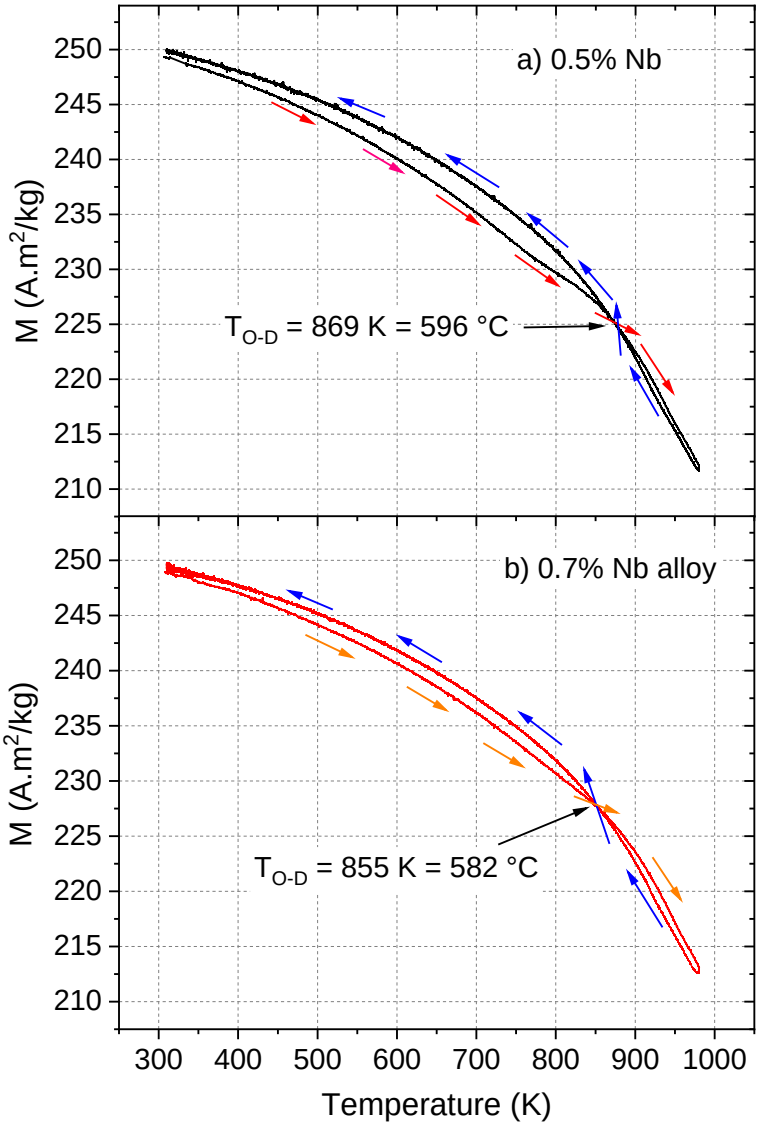

Figure 9: Magnetization as a function of temperature in the interval of 300 K to ~ 1000 K for 0.5%

Nb alloy in (a) and (b) for the 0.7% Nb alloy.

The Curie temperature T_C of Fe-Co based alloys are much higher than 1000 K. To estimate the T_Cs values of the $Fe_{65}Co_{35}$ Nb added alloys Kuz'min model is applied to the CCs. (Kuz'min, 2005). The Kuz'min model suggests that magnetization as a function of temperature can be written as Equation 1, in which different temperature ranges dependencies are built to try to fit the complete range of temperature. In Equation 1, M_0 is the M_s value at 0 K and s is a fitting parameter related to the spin wave stiffness D. The parameter p is linked to the curvature of the curve close to T_c. With the purpose of performing the fitting, the parameter p = 5 was fixed, which is a characteristic of low Co Fe-Co alloys. (Froes and Bormio-Nunes, 2024)

$$M(T) = M_0.[1 - s.(\frac{T}{T_C})^{0.5} - (1 - s).(\frac{T}{T_C})^{p}]^{0.333} \quad (1)$$

The fitted curves and the parameters extracted from the fitting are presented in Figure 8 and Table 7, respectively.

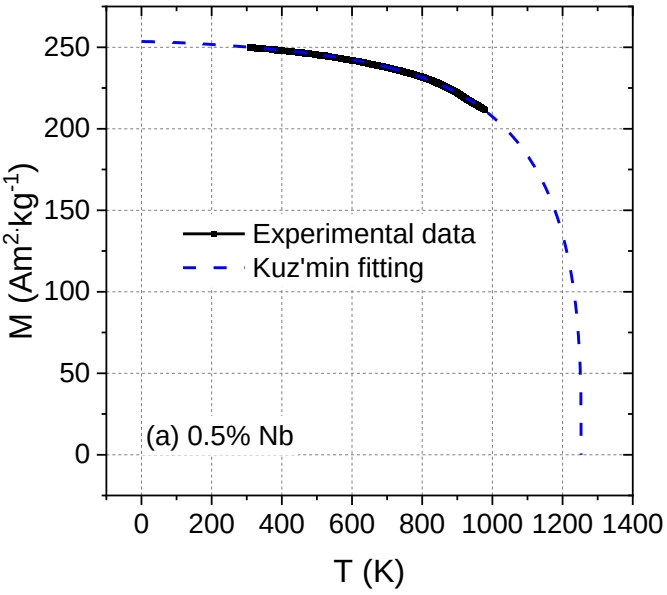

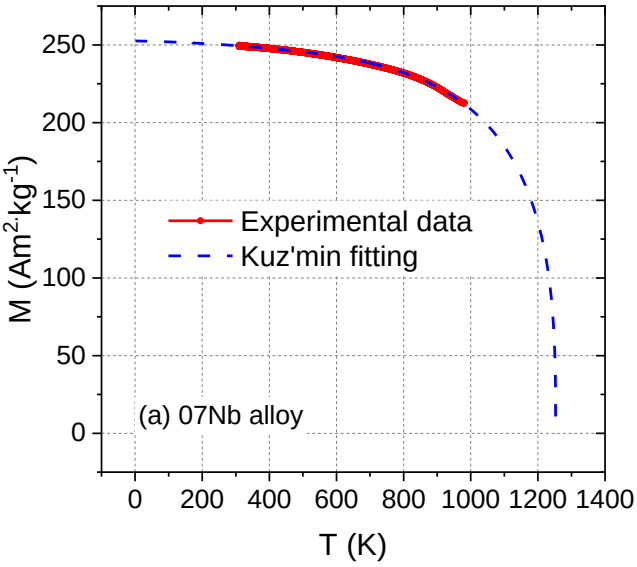

Figure 10 - Cooling magnetization vs temperature curves fitted to Kuz'min model in the interval of 300K to ~ 1000 K for 0.5% Nb alloy in (a) and (b) for the 0.7% Nb alloy

Table 7: Parameters obtained by Kuz'min model fitting

Alloy	T_C (K)	s	M_0 (A.m²/kg)
0.5% Nb-3	1253	0.33	250
0.7% Nb-3	1253	0.29	249

The calculated Curie temperature is the same for both alloys, 1243 K (970° C) and the difference of M_0 is only 1 A.m²/kg, smaller for the highest Nb content alloy, which is consistent with the difference of only 0.2% of Nb between the samples. The decrease of s is also consistent with the result of Froes and Bormio-Nunes (2024) in which addition of 1% of Nb to the alloy $Fe_{0.70}Co_{0.30}$ also caused a decrease of s from 0.30 (without Nb) to 0.27 (1% Nb) and in the present case from 0.33(0.5% Nb) to 0.29 (0.7%Nb). The parameter s may be sensitive to the solubility of Nb in the Fe-Co lattice because the

alloy $Fe_{0.70}Co_{0.30}$ has a larger lattice parameter than $Fe_{0.65}Co_{0.35}$ (Han et al., 2017). Therefore, in the alloys $Fe_{0.65}Co_{0.35}$ less quantities than 1% of Nb have almost the same effect on s than higher quantities of Nb in $Fe_{0.7}Co_{0.3}$. The solubility will affect the distance among the atoms as well as the electronic structure due to the presence of Nb, which will affect the exchange interaction J, changing D and consequently s. (Blundell, 2001) (Froes and Bormio-Nunes, 2024)

At 300K, the saturation magnetization $\mu_0 M_s$ is 2.34 T for 0.5% Nb and 2.30 T for 0.7% Nb alloy, as expected, with the added non-ferromagnetic element proportionally resulting in lower $\mu_0 M_s$ compared to 2.45 T of the binary alloy. (Sundar and Deevi, 2004) The results of $\mu_0 M_s$ are still very large and appropriate for applications.

The resistivity measurement exhibits a considerable difference in the resistivity between the two alloys, as displayed in terms of resistivity per temperature in Figure 11. The room temperature resistivity is ~ 24 $\mu\Omega$.cm for 0.5% Nb alloy and ~ 3.8 $\mu\Omega$.cm for the 0.7% Nb. In Sundar and Deevi (2005) alloys with composition in the range $Fe_{(85-65)}Co_{(15-35)}$ are mentioned to have resistivities varying in the range of 20 – 30 $\mu\Omega$.cm. A recent publication (Kozlowski et al., 2020) presents a room temperature resistivity value of 22.41 $\mu\Omega$.cm for the commercial alloy Hiperco®27 (27% Co, 0.6% Ni and Cr, 0.25% Mn and Si, 0.01% C; mass %) (Carpenter Technology, a). The resistivity of the alloy 0.5% Nb alloy is within those range mentioned in the literature, however, the resistivity of the alloy 0.7% Nb is far below. The main microstructure differences between the alloys are that 0.7% Nb alloy has a larger fraction of fraction of the C14 second phase and larger grain boundary surface. But as found in Mvs T analysis 0.7% Nb alloy has lower fraction of ordered phase than 0.5% Nb alloy.

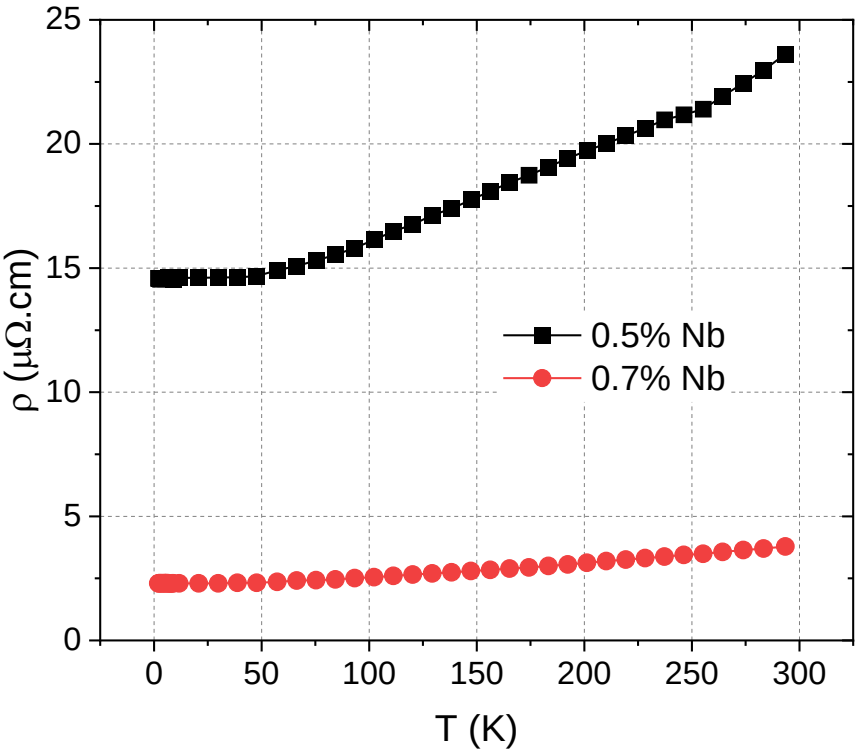

Figure 11 - Cooling resistivity vs temperature curves in the interval of 2K to ~ 300 K for 0.5% Nb alloy and 0.7% Nb alloy

The explanation of the resistivity reduction of the 0.7% Nb alloy H_c compared to the one of 0.5% alloy is consistent with the equivalent H_c behavior. The second phase (SP) and grain boundaries (GB) are less effective domain wall pinners than the deformations $\varepsilon_{O\text{-}D}$ developed between the interfaces of the ordered and disordered BCC phases in 0.7% Nb alloy because of the lower quantity of phase ordering of this material. In the same way, for the resistivity SP and GB are much less effective electron scatters than $\varepsilon_{O\text{-}D}$ in 0.7% Nb alloy, then as $\varepsilon_{O\text{-}D}(0.7\%Nb) < \varepsilon_{O\text{-}D}(0.5\%Nb) \rightarrow \rho_{O\text{-}D}(0.7\%Nb) < \rho_{O\text{-}D}(0.5\%Nb)$.

Conclusions

The addition of Nb to the $Fe_{0.65}Co_{0.35}$ alloy led to the precipitation of a $MgZn_2$ type Laves phase and a large improvement in its malleability for the 0.7% Nb addition compared to the 0.5% Nb. The magnetic properties of both alloys appoint to them as good soft materials, with high susceptibilities peaking at around 800, more than 2 times higher than the binary alloy. Relatively large coercivities values would demand further tunning in the fabrication process. The resulting Curie temperatures equates the maximum found in Fe-Co alloys in the range of 30 - 50% of Co and allows a large range of working temperatures.

Both unexpected reductions of the resistivity ρ and H_c values of the 0.7% Nb compared to the 0.5% Nb alloy are consistent was found to be a result of strains retained in the quenching of the samples from 800ºC. Those strains originate from stresses between BCC ordered and disordered phases, since 0.7%Nb alloy shows less ordering, than lower stresses and consequently lower H_c and ρ values than 0.5% Nb alloy.

Both compositions achieve similar magnetostriction, around 40 ppm, a reduced value compared to the alloy without Nb. However, those values are still high to be used in AC motors and transformers, as magnetic cores, because it would cause undesirable noise generation. Nevertheless, considering that the materials have positive and sufficiently high magnetostriction, as well as high permeability, the most relevant application niche would be as a force sensor. In subsequent study, magnetomechanical properties of the 0.5 % Nb and 0.7% Nb alloys will bring more insight for this application.

Acknowledgements

This study was mostly financed, by the São Paulo Research Foundation (FAPESP), Brazil. Processes Numbers 2021/06350-0, 2022/15334-0 and 2022/09152-7, also in part by the Coordenação de Aperfeiçoamento de Pessoal de Nível Superior - Brasil (CAPES) - Finance Code 001.

References

Bardos, D. I. (1969). Mean magnetic moments in bcc Fe–Co alloys. *Journal of Applied Physics*, *40*(3), 1371-1372. doi: <https://doi.org/10.1063/1.1657673>.

Beckley, P. (2001). Steels, Silicon Iron-based: magnetic properties. *Encyclopedia of materials: Science and Technology*, 8847-8851. doi: https://ui.adsabs.harvard.edu/link_gateway/2001emst.book.8847B/doi:10.1016/B0-08-043152-6/01590-4.

Belahcen, A. (2006). Vibrations of rotating electrical machines due to magnetomechanical coupling and magnetostriction. *IEEE Transactions on Magnetics*, *42*(4), 971-974. doi: <https://doi.org/10.1109/TMAG.2006.871469>.

Blundell, S. (2001). *Magnetism in condensed matter*. OUP Oxford.

Bormio-Nunes, C., & Froes, F. (2023). Magnetostriction reduction and magnetic permeability enhancement of Ti added Fe0. 7Co0. 3 alloy. *Journal of Applied Physics*, *133*(12). doi: < https://doi.org/10.1063/5.0140457>.

Carpenter Technology, a. Hiperco®-27. URL: <https://www. carpentertechnology.com/alloy-finder/hiperco-27>. Acessed in 27/03/2025.

Carpenter Technology, b. Hiperco®-50. URL: <https://www. carpentertechnology.com/alloy-finder/hiperco-50>. Acessed in 27/03/2025.

Cullity, B. D., & Graham, C. D. (2011). *Introduction to magnetic materials*. John Wiley & Sons.

Dias, M. B., Bormio-Nunes, C., Pacheco, C. J., de Oliveira Machado, V., & Hubert, O. (2015). Magnetomechanical behavior of a directly solidified Fe–Al–B alloy. *Smart Materials and Structures*, *24*(10), 105004. doi: <https://dx.doi.org/10.1088/0964-1726/24/10/105004>.

Froes, F., 2021. Obtenção de ligas magnéticas de fe 0,70co0,30 com adição de nb e ti: Estudo de propriedades físicas. University of São Paulo. URL: <https://www.teses.usp.br/teses/disponiveis/97/97135/tde-18012022-123336/>.

Froes, F., & Bormio-Nunes, C. (2024). High-temperature magnetization and bulk magnetostriction investigation of Ti and Nb addition to Fe70Co30 alloy. *Journal of Materials Science*, *59*(4), 1652-1664. doi: <https://doi.org/10.1007/s10853-023-09252-2>.

Gutfleisch, O., Willard, M. A., Brück, E., Chen, C. H., Sankar, S. G., & Liu, J. P. (2011). Magnetic materials and devices for the 21st century: stronger, lighter, and more energy efficient. *Advanced materials*, *23*(7), 821-842. doi: <https://doi.org/10.1002/adma.201002180>.

Han, Y., Wang, H., Zhang, T., He, Y., Coey, J. M. D., & Jiang, C. (2017). Tailoring the heterogeneous magnetostriction in Fe-Co alloys. *Journal of Alloys and Compounds*, *699*, 200-209. doi: <https://doi.org/10.1016/j.jallcom.2016.12.223>.

He, Z., Du, H., Sha, Y., Chen, S., Zhang, F., Chen, L., & Zuo, L. (2021). Secondary recrystallization behavior in magnetostrictive Fe-Ga thin sheets induced by nano-sized composite precipitates. AIP Advances, 11(3). doi: <https://doi.org/10.1063/9.0000113>.

Hocine, M., Guittoum, A., Hemmous, M., Martínez-Blanco, D., Gorria, P., Rahal, B., ... & Laggoun, A. (2017). The role of silicon on the microstructure and magnetic behaviour of nanostructured (Fe0. 7Co0. 3) 100− xSix powders. Journal of Magnetism and Magnetic Materials, 422, 149-156. doi: <https://doi.org/10.1016/j.jmmm.2016.08.058>.

Kawahara, K. (1983). Effect of additive elements on cold workability in FeCo alloys. *Journal of Materials Science, 18,* 1709-1718. doi: <https://doi.org/10.1007/BF00542066>.

Khomenko, M. R., Pankratov, N. Y., Karpenkov, A. Y., Karpenkov, D. Y., Tereshina, I. S., & Nikitin, S. A. (2023). Structural and magnetostrictive properties of intermetallic (Tb, Ho)(Fe, Co) 2 compounds. *Physica B: Condensed Matter*, *669*, 415198. doi: <https://doi.org/10.1016/j.physb.2023.415198>.

Kozlowski, G., Susner, M. A., Horwath, J. C., & Turgut, Z. (2020). Thermal transport properties of Fe–Co alloys. *Continuum Mechanics and Thermodynamics*, *32*(1), 247-254. doi: <https://doi.org/10.1007/s00161-019-00800-3>

Kurita, H., binti Fakhruddin, S. M., Inoue, K. Y., Nakaki, T., Kuroda, S., Wang, Z., ... & Narita, F. (2023). Energy-harvesting and mass sensor performances of magnetostrictive cobalt ferrite-spattered Fe–Co alloy plate. *Journal of Alloys and Compounds*, *951*, 169844. doi: <https://doi.org/10.1016/j.jallcom.2023.169844>.

Kuz'min, M. D. (2005). Shape of Temperature Dependence of Spontaneous Magnetization of Ferromagnets: Quantitative Analysis. *Physical review letters*, *94*(10), 107204. doi: <https://doi.org/10.1103/PhysRevLett.94.107204>.

Muralles, M., Oh, J. T., & Chen, Z. (2024). Atomistic investigation of effect of alloying on mechanical properties and microstructural evolution of ternary FeCo-X (X= V, Nb, Mo, W). *Computational Materials Science*, *241*, 113030. doi: <https://doi.org/10.1016/j.commatsci.2024.113030>.

Ohnuma, I., Enoki, H., Ikeda, O., Kainuma, R., Ohtani, H., Sundman, B., & Ishida, K. (2002). Phase equilibria in the Fe–Co binary system. *Acta Materialia*, *50*(2), 379-393. doi: < https://doi.org/10.1016/S1359-6454(01)00337-8>.

Paduani, C., Schaf, J., Persiano, A. I. C., Ardisson, J. D., Takeuchi, A. Y., & Raposo, M. T. (2009). Evidence of weak ferromagnetism in the C14 Laves phase (Fe1− xCox) 2Nb system. *Journal of alloys and compounds*, *474*(1-2), 34-37. doi: <https://doi.org/10.1016/j.jallcom.2008.06.119>.

Silva, I. B., Froes, F., Ferreira, H. N. A., Hubert, O., & Bormio-Nunes, C. (2024, May). Piezomagnetism in Cr Dopped Fe 65 Co 35 Alloy. In *2024 IEEE International Magnetic Conference-Short Papers (INTERMAG Short Papers)* (pp. 1-2). IEEE. doi: 10.1109/INTERMAGShortPapers61879.2024.10576837.

Sundar, R. S., & Deevi, S. C. (2005). Soft magnetic FeCo alloys: alloy development, processing, and properties. *International materials reviews*, *50*(3), 157-192. doi: <https://doi.org/10.1179/174328005X14339>.

Sundar, R. S., & Deevi, S. C. (2004). Influence of alloying elements on the mechanical properties of FeCo–V alloys. *Intermetallics*, *12*(7-9), 921-927. doi: <https://doi.org/10.1016/j.intermet.2004.02.022>.

TRADING ECONOMICS, URL: <https://tradingeconomics.com/commodities>. Accessed in 27/03/2025.

Ustinovshikov, Y. I., Pushkarev, B. E., & Sapegina, I. V. (2006). Phase separation and ordering in the Fe-Co system. *Inorganic materials*, *42*, 354-359. doi: <https://doi.org/10.1134/S0020168506040042>.

Varli, K. V., Druzhinina, T. I., D'yakonova, N. P., Pirogova, S. E., & Rutman, A. M. (1981). Effect of cobalt and nickel alloying on stability of phases of Fe-Nb system. *Izv. Vyssh. Uchebn. Zaved., Chern. Metall.;(USSR)*, *9*. URL: <https://www.osti.gov/etdeweb/biblio/7088601>.

Xu, J., Peng, X., Li, J., Wang, X., & Hong, B. (2024). Comparative study in magnetic properties of

FeCo alloy nanowires and a first-order reversal curve analysis. *Journal of Magnetism and Magnetic Materials, 608,* 172444. doi: <https://doi.org/10.1016/j.jmmm.2024.172444>.

Yamazaki, T., Furuya, Y., Hata, S., & Nakao, W. (2021). Stress-driven magnetic Barkhausen noise generation in FeCo magnetostrictive alloy. *IEEE Transactions on Magnetics*, *58*(1), 1-8. https://doi.org/10.1109/TMAG.2021.3126898. doi: 10.1109/TMAG.2021.3126898.

Zhang, R., Zhou, C., Chen, K., Cao, K., Zhang, Y., Tian, F., ... & Song, X. (2021). Near-zero magnetostriction in magnetostrictive FeCo alloys. *Scripta Materialia, 203,* 114043. doi: <https://doi.org/10.1016/j.scriptamat.2021.114043>.

.